



HAL
open science

Rampant Genome-Wide Admixture across the Heliconius Radiation

Krzysztof M Kozak, Mathieu Joron, W Owen Mcmillan, Chris D Jiggins

► **To cite this version:**

Krzysztof M Kozak, Mathieu Joron, W Owen Mcmillan, Chris D Jiggins. Rampant Genome-Wide Admixture across the Heliconius Radiation. *Genome Biology and Evolution*, 2021, 13 (7), pp.evab099. 10.1093/gbe/evab099 . hal-03451709

HAL Id: hal-03451709

<https://hal.science/hal-03451709>

Submitted on 26 Nov 2021

HAL is a multi-disciplinary open access archive for the deposit and dissemination of scientific research documents, whether they are published or not. The documents may come from teaching and research institutions in France or abroad, or from public or private research centers.

L'archive ouverte pluridisciplinaire **HAL**, est destinée au dépôt et à la diffusion de documents scientifiques de niveau recherche, publiés ou non, émanant des établissements d'enseignement et de recherche français ou étrangers, des laboratoires publics ou privés.

Rampant Genome-Wide Admixture across the *Heliconius* Radiation

Krzysztof M. Kozak ^{1,2,*}, Mathieu Joron³, W. Owen McMillan^{1,†}, and Chris D. Jiggins^{1,2,†}

¹Smithsonian Tropical Research Institute, Panamá, Panamá

²Department of Zoology, University of Cambridge, United Kingdom

³Centre d'Ecologie Fonctionnelle et Evolutive (CEFE), CNRS, Université de Montpellier, Université Paul Valéry Montpellier 3, EPHE, IRD, France

*Corresponding author: E-mail: evoecogen@gmail.com.

Accepted: 30 April 2021

†These authors contributed equally to this work.

Abstract

How frequent is gene flow between species? The pattern of evolution is typically portrayed as a phylogenetic tree, yet gene flow between good species may be an important mechanism in diversification, spreading adaptive traits and leading to a complex pattern of phylogenetic incongruence. This process has thus far been studied mainly among a few closely related species, or in geographically restricted areas such as islands, but not on the scale of a continental radiation. Using a genomic representation of 40 out of 47 species in the genus, we demonstrate that admixture has played a role throughout the evolution of the charismatic Neotropical butterflies *Heliconius*. Modeling of phylogenetic networks based on the exome uncovers up to 13 instances of interspecific gene flow. Admixture is detected among the relatives of *Heliconius erato*, as well as between the ancient lineages leading to modern clades. Interspecific gene flow played a role throughout the evolution of the genus, although the process has been most frequent in the clade of *Heliconius melpomene* and relatives. We identify *Heliconius hecalesia* and relatives as putative hybrids, including new evidence for introgression at the loci controlling the mimetic wing patterns. Models accounting for interspecific gene flow yield a more complete picture of the radiation as a network, which will improve our ability to study trait evolution in a realistic comparative framework.

Key words: admixture, adaptive introgression, radiation, phylogenomics.

Significance

Gene flow and adaptive introgression have been documented across the tree of life, but the overall importance of these processes for the diversity of life remains unclear. We find that admixture between species has been common during the evolution of *Heliconius* butterflies, and was the mechanism spreading multiple advantageous genes. Therefore, we point to gene flow between species as a key force shaping an adaptive radiation.

Introduction

Interspecific hybridization and the resulting gene flow across porous species barriers are increasingly recognized as major processes in evolution, detectable across the tree of life (Hilario and Gogarten 1993; Feliner et al. 2017). Interspecific gene flow has since been demonstrated in several animal taxa, both at deep (Chen et al. 2017) and shallow temporal scales (e.g., Fontaine et al. 2015). Although

hybridization might often result in the production of deleterious combinations of alleles at different loci, introgression can also enable adaptation by providing novel variation that may be favored by natural selection, as demonstrated in the iconic adaptive radiation of Darwin's finches (Lamichhaney et al. 2015) and in our own lineage (Huerta-Sánchez et al. 2014).

The task ahead is to systematically evaluate the prevalence and importance of interspecific gene flow in fueling

© The Author(s) 2021. Published by Oxford University Press on behalf of the Society for Molecular Biology and Evolution.

This is an Open Access article distributed under the terms of the Creative Commons Attribution License (<http://creativecommons.org/licenses/by/4.0/>), which permits unrestricted reuse, distribution, and reproduction in any medium, provided the original work is properly cited.

speciation in adaptive radiations (Schumer et al. 2014; Feliner et al. 2017). Unfortunately, modeling gene flow requires extensive data and poses greater challenges to computational methods than other processes leading to incongruent signals, such as incomplete lineage sorting or gene duplication (Degnan 2018; Wen et al. 2018). For instance, two studies of the swordtail fishes applied different sequencing and analytical strategies, ultimately reaching dissimilar conclusions on the prevalence of hybridization in *Xiphophorus* (Cui et al. 2013; Kang et al. 2013). The challenge of characterizing introgression in adaptive radiations remains open and requires both taxonomic completeness and sophisticated methodological approaches.

The Neotropical *Heliconius* butterflies present an excellent opportunity to study the incidence and importance of gene flow in a recent adaptive radiation, due to the natural propensity of *Heliconius* and the sister genus *Eueides* to produce hybrids in the wild (Dasmahapatra et al. 2007; Mallet et al. 2007). The loci responsible for their aposematic wing patterns are especially likely to be shared between species, providing a source of genetic variation in a strongly selected trait and thus likely facilitating speciation (*Heliconius* Genome Consortium 2012; Pardo-Diaz et al. 2012; Enciso-Romero et al. 2017; Jay et al. 2018; Edelman et al. 2019; Massardo et al. 2020) (summarized in [supplementary table 1, Supplementary Material](#) online). In the so called *melpomene/cydnio/silvaniform* clade (MCS), species in sympatry can share variation at up to 40% of the genome (Kronforst et al. 2013; Martin et al. 2013).

It remains unknown whether hybridization and introgression documented in the relatively young MCS clade (4.5–3.5 Ma) (Kozak et al. 2015) are a universal characteristic of this genus. Recent studies of the genus *Heliconius* based on de novo assembly of genomes (Edelman et al. 2019 Seixas et al., 2021) and transcriptomes (Zhang et al. 2019) have identified instances of admixture in other groups, but looked at single individuals in less than half of the 47 recognized species. Furthermore, a study of *Heliconius hermathena* revealed that a phenotype suggestive of introgression is in fact determined by an ancestral allele expressed in multiple species (Massardo et al. 2020). Full understanding of the frequency of interspecific admixture events requires comprehensive analysis across the diverse species and phenotypic races in the genus.

Here, we generate a comprehensive whole-genome resequencing data set of 145 individuals of 40 among the 47 recognized *Heliconius* species, and six out of 12 *Eueides*, encompassing nearly an entire radiation at a continental scale (fig. 1 and [supplementary file 1, Supplementary Material](#) online). With this expanded data set, we investigate the prevalence of hybridization, attempt to quantify its extent across the radiation, and compare the processes producing discordance. We demonstrate varied amounts of phylogenetic incongruence (i.e., conflict between gene trees [Degnan 2018] related to heterogenous levels of gene flow among species). We show that a misleadingly well-supported and resolved

tree can be recovered despite incongruence, and that previously unknown, complex hybridization events can thus be missed. Although instances of hybridization across the genome, particularly at adaptive loci, are found across the radiation, we demonstrate that they are far more frequent among the relatives of *Heliconius melpomene*.

Results

Genomic Trees for the Heliconiines

We first constructed a bifurcating autosomal phylogeny. Mapping genome-wide short read data from 145 individuals in 48 species ([supplementary file 1](#) and [table 3, Supplementary Material](#) online) to the *H. melpomene* reference allowed us to recover 6,848 autosomal and 416 sex-linked high quality, orthologous CDS alignments, respectively (of which 6,725 and 406 include at least one outgroup sequence). The mean length of a quality-trimmed autosomal alignment was 1,387 base pairs ([supplementary table 4, Supplementary Material](#) online), and the average parametric aLRT support for the estimated maximum likelihood gene trees was 0.675 ± 0.060 with all samples included. Filtering for autosomal exome sites with biallelic, nonsingleton SNPs without missing data produced a 122,913 bp supermatrix. This underpins a maximum likelihood tree resolved with full bootstrap support, except for uncertain placement of the *Heliconius clysonymus/hortense/telesiphe* clade (bootstrap support 62/100), which is also placed differently in the coalescent analyses (fig. 1 and [supplementary fig. 1, Supplementary Material](#) online). ASTRAL-III and MP-EST, which infer the species tree from gene trees, also yield highly resolved and supported phylogenies (fig. 1 and [supplementary fig. 2, Supplementary Material](#) online). The multispecies coalescent (MSC) trees differ from each other at only two relatively recent splits out of 56. The concatenation phylogeny differs from the ASTRAL at three nodes, and from MP-EST at two (fig. 1).

Genome-Wide Incongruence and Discordance

Although the species tree topologies recovered by various approaches from the autosomal markers are very similar, multiple indices show incongruence among individual gene trees. The Robinson–Foulds pairwise distance is high: 0.745 out of 1.0 for the autosomal phylogenies and 0.699 for the sex-linked loci, indicating that any two gene trees are very likely to contain multiple differing nodes. Among the 56 nodes separating species and major subspecies, less than a half (26) are resolved in an autosomal majority rule consensus tree ([supplementary fig. 4, Supplementary Material](#) online). The relative tree certainty (Salichos et al. 2014) on a 0–1 scale is a low 0.322 when using all gene trees, and increases to 0.397 for the 1,000 best gene trees. Many branches with high support in the coalescent trees score low on the internode certainty (IC) measures (IC/ICA; [supplementary fig. 4, Supplementary Material](#) online). Brower and

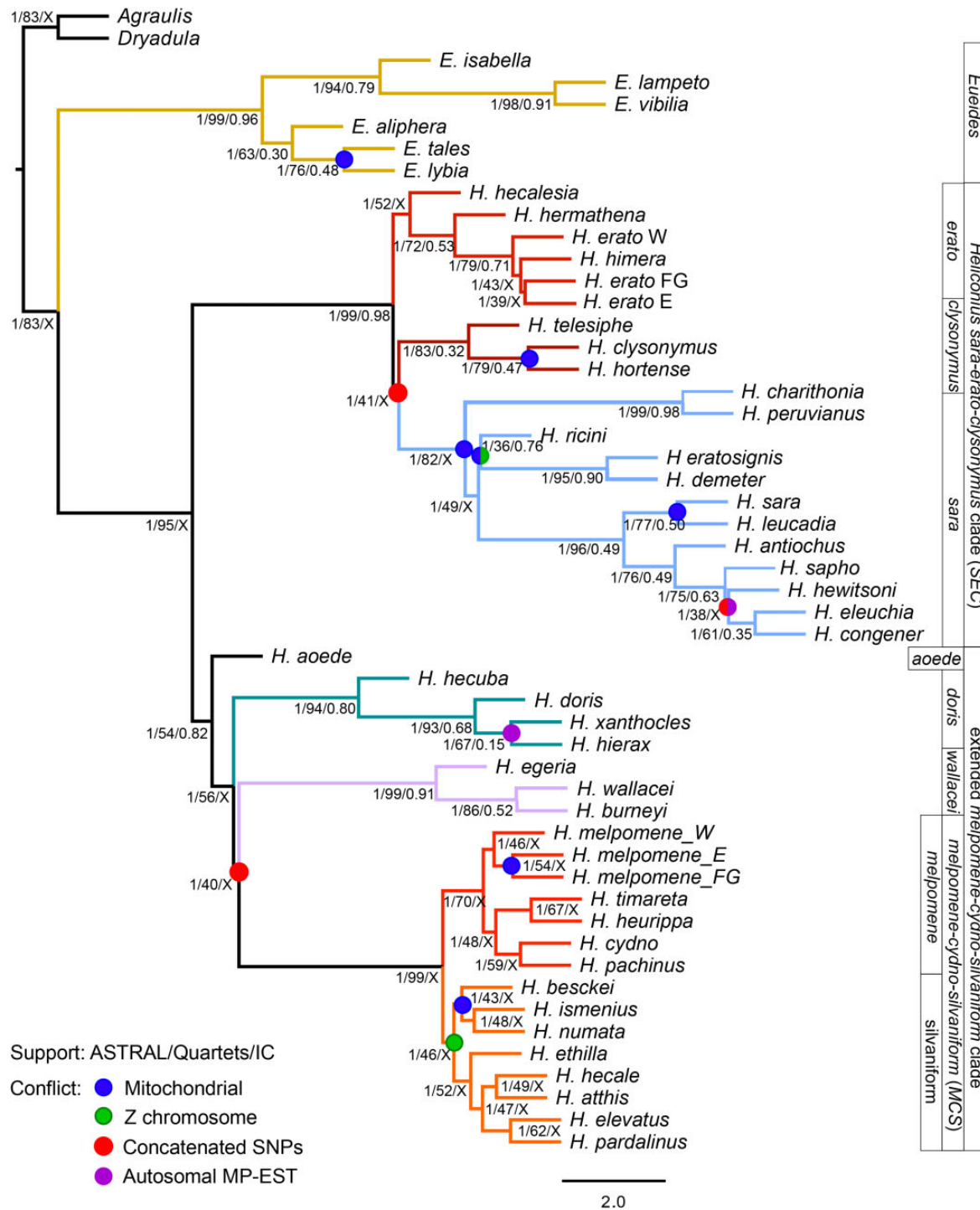


FIG. 1.—Bifurcating model of Heliconiini phylogeny obscures the underlying incongruence. The topology was inferred by the multispecies coalescent method ASTRAL-III from 6,725 orthologous autosomal genes. All nodes, except for the *CHT* clade are supported in 100% bootstrap replicates. In addition, three types of support values are presented: ASTRAL branch support for a quadripartition (on a 0–1 scale); percentage of quartets in individual gene trees containing a specific node; and the Internode Certainty measure of gene tree incongruence (0–1 scale; X indicates the node is not found in the consensus). Colored circles indicate conflict between the topology of the ASTRAL autosomal tree, and the estimates from: mitochondrial data under ML (blue); sex-linked genes (Z chromosome) in ASTRAL under ML (red); the alternative coalescent method MP-EST (violet). Branch lengths are in coalescent units, and arbitrarily set to 1.0 for the terminal branches. Branch colors correspond to previously defined clades (Kozak et al. 2015): red—*Heliconius melpomene/cydnosilvaniform* (MCS); violet—*Heliconius wallacei*; green—*Heliconius doris*; blue—*Heliconius sara*; crimson—*Heliconius clysonymus*; scarlet—*Heliconius erato*; brown—*Eueides*.

Garzón-Orduña (2018) suggested that incongruence reported previously (Kozak et al. 2015) was an artifact of missing data. Here, we present nucleotide matrices that are nearly complete (>96%). Although modern statistical phylogenetic methods are typically robust to far higher levels of missing data (Wiens and Morrill 2011; Roure et al. 2013), we still find substantial discordance and incongruence, which shows they are not merely artifacts.

Conflicts are further highlighted by the varied quartet support, whereby many of the nodes reported as certain by ASTRAL are only found in a fraction of the gene trees (second set of support values in fig. 1). This discrepancy is especially exacerbated in the low quartet support for the position of species in the MCS clade, as well as at the placement of the small clades of *Heliconius aoede*, *Heliconius wallacei*, *Heliconius doris*, and *H. clysonymus*. The statistics are not strongly affected by the exact choice of markers. When the 6,367 single exons are used instead of entire genes, the total normalized quartet score for the entire ASTRAL tree decreases only slightly from 0.847 to 0.806, while the quartet support of individual nodes changes by no more than 10 percentage points (supplementary fig. 3, [Supplementary Material](#) online).

We found that the Z chromosome gene trees are more congruent with each other (supplementary figs. 5 and 6, [Supplementary Material](#) online) and more concordant with the coalescent species trees (supplementary figs. 7 and 8, [Supplementary Material](#) online), than are the autosomal trees (Wilcoxon's test, $P = 3 \times 10^{-11}$). Notably, many nodes within the MCS clade are resolved among the Z chromosome trees, and the *H. melpomene/cydno* group is monophyletic (supplementary fig. 4, [Supplementary Material](#) online), unlike in the consensus of autosomal gene tree topologies, where it is mixed with silvaniform relatives (supplementary fig. 4, [Supplementary Material](#) online). Similarly, the whole mitochondrial phylogeny was both well-supported, and conflicted with the MSC trees at different levels of divergence (fig. 1 and supplementary fig. 9, [Supplementary Material](#) online).

Hybridization between Species Has Been Common throughout the Radiation of *Heliconius*

For the first time, we test for gene flow across the entire radiation, including nearly all species ($N = 27$) in clades other than the previously studied MCS ($N = 13$). Across the radiation, an inference of species networks reveals a pattern of gene sharing within all major clades of the radiation (figs. 2 and 3 and [supplementary file 3, Supplementary Material](#) online). Both the coalescent network (PhyloNet, fig. 2A) and the admixture graph (AG) (TreeMix, fig. 3) support the known gene flow between East Andean races of *H. melpomene* and *Heliconius heurippa/Heliconius timareta* (figs. 2 and 3, edge 1), as well as between the Western races of *H.*

melpomene and *Heliconius cydno/Heliconius pacheus* (fig. 3, edge 2). The inferred admixture edges show gene flow at a substantial proportion of the surveyed loci (corresponding to the inheritance probability γ ; Zhang et al. 2019): 0.34 for *H. melpomene/H. cydno* and 0.22 *H. melpomene–H. timareta*. Both methods show gene flow between silvaniforms and the *H. melpomene/cydno* clade, although compared with the MPL network, the AG suggests more events at a larger proportion of the loci (fig. 3, edges 3–5). Conversely, the network contains more admixture events in the deeper past.

Ample evidence is found for gene flow among other clades and in the deeper past. Gene flow with inheritance probabilities of 0.39 is inferred between MCS, and both clades of *H. wallacei* and *H. doris* (fig. 2A), along extensive gene flow within the latter two clades. The two inference methods suggest large disagreement on the placement of *H. aoede* ($\gamma = 0.40$, fig. 2A), but suggest gene flow either from *H. aoede* to the *Heliconius hecuba* clade (AG), or a “ghost lineage” linked to a clade of *H. aoede* and MCS (MPL). Finally, the most likely network estimated for the genus *Eueides* contains three reticulations (supplementary fig. 10, [Supplementary Material](#) online), all of which connect to a “ghost taxon” (Wen et al. 2018).

Mosaic Genomes in the *Heliconius erato* Clade

Proportionally fewer admixture events are identified in the network of the SEC clade (three interspecific admixture edges among 21 lineages; fig. 2B) than among other *Heliconius* (10 edges between 23 lineages). Nonetheless, support for admixture in this lineage is strong as well. In particular, *Heliconius hecalesia* shares a large portion of its genome with either the ancestor of the (*H. telesiphe*, (*hortense*, *clysonymus*)) clade ($\gamma = 0.38$, fig. 2B), or just with *H. clysonymus* ($\gamma = 0.16$). Furthermore, there is some evidence for an exchange between the CHT and *Heliconius sara* clades ($\gamma = 0.06$). The TreeMix AG also uncovers the CHT-*H. hecalesia* admixture, but places both in different positions in the tree, such that *H. hecalesia* appears more closely related to the *H. sara* clade, and admixes with both CHT and *H. erato* (fig. 3, edges 6 and 7). Although grouped with *H. erato* in simple trees (figs. 1–3), *H. hecalesia* appears to be nearly equally diverged from the clades of *H. erato* and *H. clysonymus* (fig. 4A), and the support for the placement of *H. hecalesia* with either lineage is nearly equivocal among individual gene trees (quartet score 52/100). Similarly, the position of the CHT triplet, often placed with *H. hecalesia*, is the only unsupported branch in the autosomal ML phylogeny (fig. 1 and supplementary fig. 1, [Supplementary Material](#) online). No definite placement of *H. hecalesia* and the CHT clade is found in a majority of gene trees, as evidenced by consensus and DensiTree plots (IC = 0; supplementary figs. 4 and 11, [Supplementary Material](#) online).

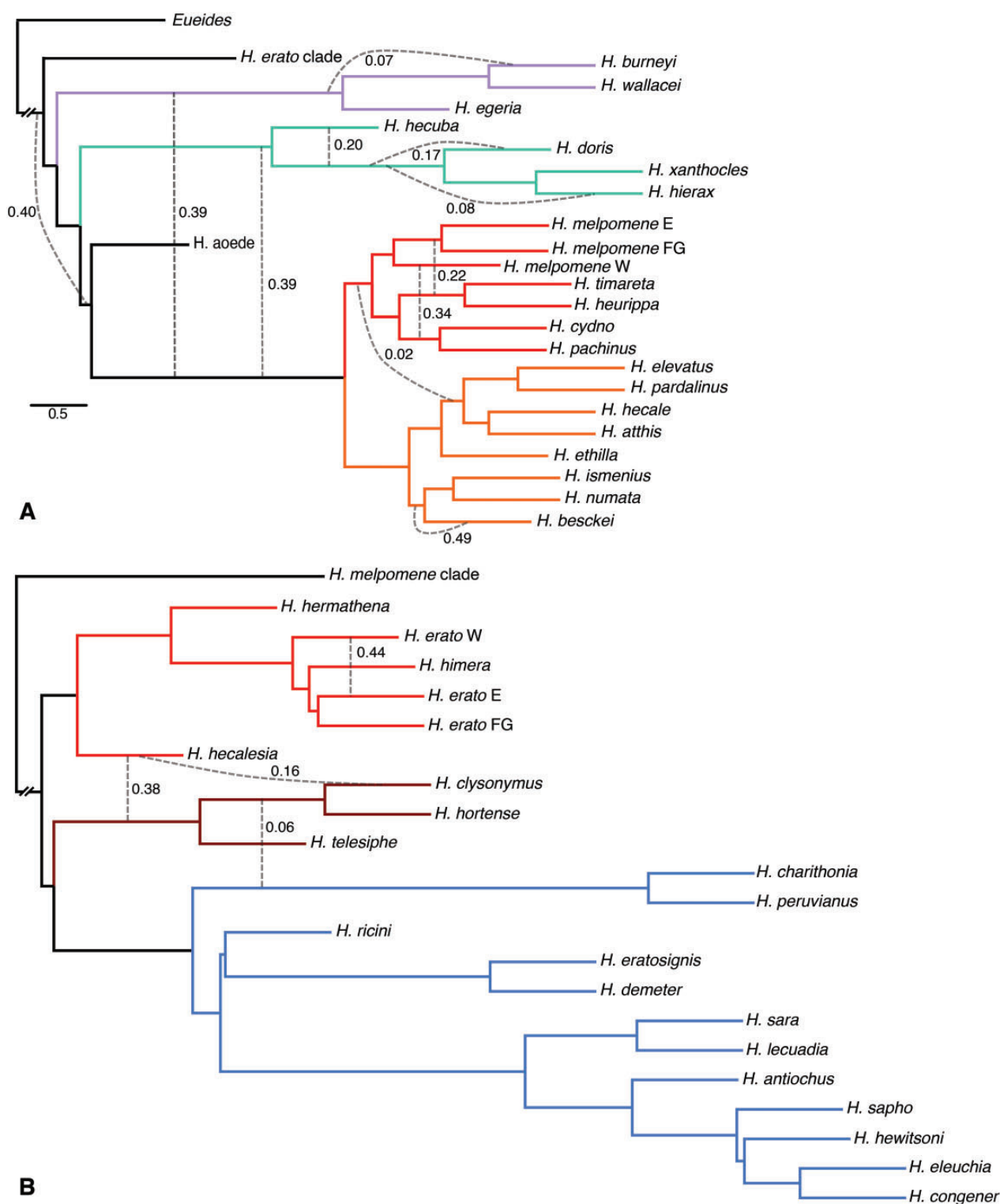


FIG. 2.—Evidence of introgression is found across the entire *Heliconius* radiation. Networks inferred under maximum pseudolikelihood (MPL) based on 6,725 autosomal ML gene trees distinguish between introgression and incomplete lineage sorting, revealing several admixture events. Numbers on the edges indicate the inheritance probabilities (Wen et al. 2018), which correspond to the proportion of the data supporting the grouping. (A) The analysis of *Heliconius melpomene* and cognates reveals previously undetected introgressions closer to the root of the tree. Known events in the MCS clade are recapitulated, demonstrating sensitivity of the approach. (B) Fewer admixtures occurred in the evolution of the *Heliconius erato/sara* clade, but *Heliconius hecalesia* may be a recent hybrid.

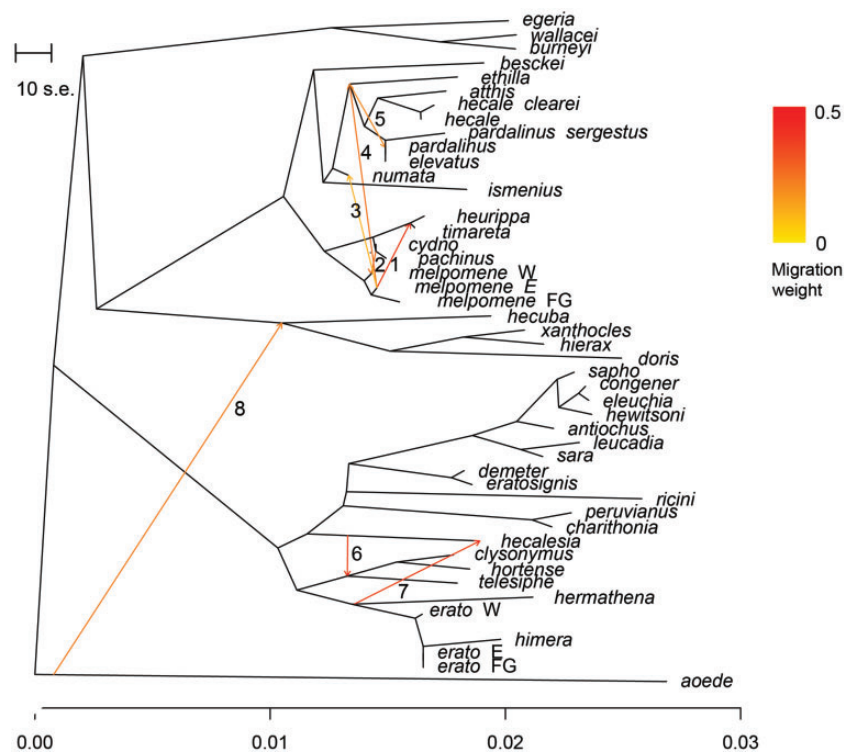


Fig. 3.—The extent of interspecific gene flow varies across the tree. TreeMix inference of splits and mixture from autosomal SNPs. Migration edges (1–8) are inferred on a phylogenetic tree built from allele frequencies under a Gaussian genetic drift approximation. Colors of the edges correspond to the proportion of the genome exchanged.

The admixture during in the evolution of *H. hecalesia* and the *CHT* clade is evident in the pattern of variation among rooted triplets of taxa, examined using the *D* statistic (Durand et al. 2011) (table 1). The results are highly positive and statistically significant for all tests where *H. hecalesia* is the recipient of admixture from either the *H. clysonymus* or *H. sara* clades (table 1). However, consistent with the phylogenetic patterns, there is evidence for stronger gene flow between *H. hecalesia* and *H. clysonymus* ($D = 0.35$; $P < 0.0001$) or *H. hortense* ($D = 0.38$; $P < 0.0001$) than the very differently patterned *H. sara* ($D = 0.17$; $P < 0.0001$).

Explicit coalescent modeling also favors models where admixture occurs across species boundaries (fig. 4B–E). In general, these models are consistent with the network and the AG. Specifically, the *CHT* clade is at the nexus of admixture events, exchanging alleles with *H. erato* and *H. hecalesia* (fig. 4B and C); *H. sara* (fig. 4D); and *Heliconius charithonia* (fig. 4E). For each triplet, one model with gene flow was strongly preferred ($wAIC = 1$), although the inferred rate of gene flow between lineages is a low value of $0.1 4Nm$, not showing any of the variation in the amount of admixture reflected by the network γ values. The estimates of divergence times are inconsistent between models, as the inferred time of coalescence between *CHT* and the sister clade of *H. sara* varies with the exact choice of species (fig. 4D vs. E).

Adaptive Introgression at the Wing Pattern Loci

Our nearly exhaustive sampling of *Heliconius* species provides a uniform framework in which to gauge the amount of introgression across the functionally important loci that modulate adaptive phenotypic variation. Topologies around wing pattern loci differ from the species tree ($P < 0.001$, SH test) and in many cases, primarily at the *optix* and *cortex* loci, show multiple departures (supplementary table 5, Supplementary Material online). The majority of the differences are found in the *MCS* clade, where introgression reaches considerable complexity across genomic and geographic regions (Wallbank et al. 2016; Enciso-Romero et al. 2017). Among *Eueides* and in the small clades of *H. aoede*, *H. doris*, and *H. wallacei*, there is no discordance observed at the pattern loci (e.g., fig. 5), despite evidence for gene flow in other parts of the genome (figs. 2 and 3).

The clustering of *H. hecalesia* and *H. clysonymus*/*H. hortense* is the only case where there is strong evidence for adaptive introgression among the 19 species of the *SEC* clade. Sequences from the three species indeed cluster exactly at the 360,000:380,000 interval of scaffold HE670865 ($aLRT > 0.95$; $P < 0.001$, SH test), which aligns to the specific region of the *optix* locus controlling red patterns in *H. erato* (Supple et al. 2013) (fig. 5). This indicates that the alleles governing the red pattern in the three species are more similar than expected from the autosomal phylogenies. *H. hecalesia*/

Table 1

D-Statistic Values (ABBA/BABA Tests) of Admixture between *Heliconius hecalesia* and Relatives

<i>P</i> ₁	<i>P</i> ₂	<i>P</i> ₃	<i>D</i>	Error(<i>D</i>)	<i>P</i> value
<i>erato</i> FG	<i>hecalesia</i>	<i>clysonymus</i>	0.349	0.009	<0.0001
<i>erato</i> FG	<i>hecalesia</i>	<i>hortense</i>	0.383	0.009	<0.0001
<i>erato</i> FG	<i>hecalesia</i>	<i>telesiphe</i>	0.269	0.008	<0.0001
<i>erato</i> FG	<i>hecalesia</i>	<i>charithonia</i> + <i>peruvianus</i>	0.208	0.005	<0.0001
<i>erato</i> FG	<i>hecalesia</i>	<i>sara</i> + <i>leucadia</i>	0.170	0.005	<0.0001
<i>erato</i> East	<i>hecalesia</i>	<i>clysonymus</i>	0.354	0.009	<0.0001
<i>erato</i> East	<i>hecalesia</i>	<i>sara</i> + <i>leucadia</i>	0.178	0.004	<0.0001

NOTE.—*P*₂ and *P*₃ are the taxa hypothesized to exchange variants, while the outgroup is always *Heliconius melpomene*. Positive *D* values are evidence for admixture after accounting for ILS. The tests are performed on autosomal SNPs and *P*-values are calculated by block jackknifing.

clysonymus/hortense cluster also at the *wntA* interval (HE667780: 450,000:490,000) (Martin et al. 2012), to the exclusion of the phenotypically more different *H. telesiphe*.

Considering the heterogeneity observed at the rest of the genome, the discordance in the regions associated with wing patterning may be a product of ILS and not hybridization. We tested this possibility by comparing Bayesian species tree and species network models. At an interval within the *optix* locus (i.e., red patterns; table 2), we find strong support for the network model over the simple tree model (Bayes Factor = 242), and 99.8% of the posterior estimates are networks with at least one admixture edge ($\mu = 3.92$, $\sigma = 1.47$). However, the posterior includes 480 topologies, the most common found only in 11.64% of the posterior. This topology (supplementary fig. 12, Supplementary Material online) implies six incidences of gene flow throughout the *SEC* clade, and places *H. hecalesia* in a soft polytomy in the *CHT* clade. In addition, the inferred age of the *CHT* clade (1.6–1.4 Ma; supplementary fig. 12, Supplementary Material online) is much lower than expected from a relaxed molecular clock estimate (4.5–2.7 Ma) (Kozak et al. 2015). Although this discrepancy could be caused by the use of a strict clock here, all the other split times are consistent between the strict and relaxed clock estimates.

At the *Cr* interval (*cortex*: yellow patterns), there is similarly overwhelming support for a network structure over a tree (BF = 411), and 99.4% of the posterior are networks with an average of 3.24 reticulations ($\sigma = 1.54$). Unexpectedly, the most frequent topology (7.86%; supplementary fig. 13, Supplementary Material online) does not place *H. charithonia* with *H. sara*, and contains a single admixture from the ancestor of the *CHT* clade. At *wntA* (the shape locus) the preferred model is also a network (Bayes Factor = 28), and 99.1% of all posterior estimates contain admixture edges ($\mu = 2.58$, $\sigma = 1.98$). Among the most probable networks in the Bayesian posterior, *H. hecalesia* is placed with the *CHT* clade, and 75% of the networks imply gene flow between this clade and *H. charithonia* (supplementary fig. 14, Supplementary Material online).

In the *MCS* clade, in addition to corroborating previous reports of introgression around color pattern regions, we identify several new cases. For instance, at the *cortex* locus (see table 2), which is responsible for the diverse white and yellow patterns across the genus (Nadeau et al. 2016), *H. melpomene* and *H. timareta* alleles cluster with silvaniforms (scaffold HE667780:310,000:330,000; aLRT > 0.95). At the *wntA* locus (HE668478:450,000:490,000), sequences of *H. heurippa* cluster with *H. cydno*, upholding the view that speciation of the former involved a yellow-patterned race of *H. cydno* (Enciso-Romero et al. 2017), although the rest of the data places *H. heurippa* unequivocally as sister to *H. timareta* (figs. 1–3). Most of the variation in the *optix* region is consistent with the genome-wide lack of resolution in the *H. melpomene/cydno/silvaniform* clade and confirms known events. The greatest number of discordant branches are among the *H. melpomene/cydno* clade at 360,000:380,000 (fig. 5), the section controlling both *H. melpomene* (Wallbank et al. 2016) and *H. erato* red ray patterns (Supple et al. 2013; Van Belleghem et al. 2017). Intriguingly, alleles from *H. hecale clearei* cluster with the *Heliconius pardalinus/Heliconius elevatus* sequences in eight out of 60 windows on the *optix* scaffold, perhaps related to the complete loss of orange patterning in this uniquely black and white silvaniform (fig. 5).

Discussion

In-Depth Sampling Reveals Widespread Admixture

We interrogated an extensive data set of 6,725 autosomal genes sequenced in nearly all species of a continental-scale adaptive radiation to investigate the prevalence of genome-wide admixture. We identified up to 13 cases of gene flow between species as a major source of phylogenetic incongruence (fig. 2), and demonstrated that admixture shaped the evolution of *Heliconius* throughout their history. Coalescent modeling revealed admixture between deeply diverged lineages, as well as a complex history of gene flow in the *SEC* clade of the genus. Although *Heliconius* is recognized as a foremost example of interspecific gene flow, most of the studies (reviewed in supplementary table 1, Supplementary Material online) focused on *H. melpomene* and relatives, known to hybridize in the wild with notable frequency (Mallet et al. 2007). Recent studies highlighted new cases in other clades within the genus (Edelman et al. 2019; Zhang et al. 2019), but limited taxonomic and geographic representation of *Heliconius* diversity made it difficult to assess reliably how many species have admixed (Thawornwattana et al. 2021). Here, we include 40/47 species and highlight the importance of admixture in shaping this complex radiation across time. We used the previously investigated clade of *H. melpomene*, *H. cydno* and silvaniforms as a test case, where our approach supports other work documenting extensive admixture, including: hybridization during speciation of *H.*

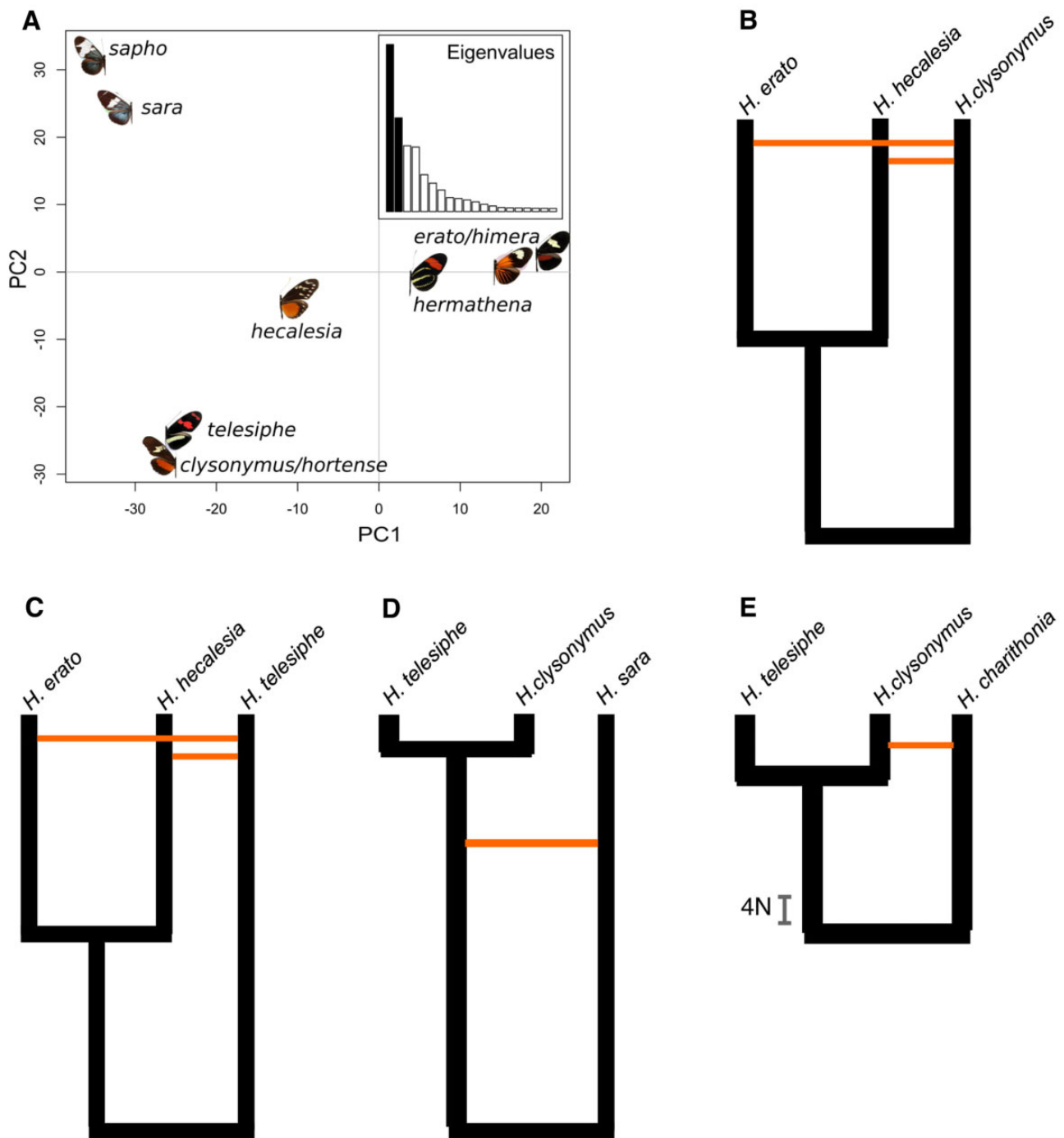


FIG. 4.—Ambiguous genomic composition of *Heliconius hecalesia*. (A) Although usually recovered as the sister species of *Heliconius hermathena* and *Heliconius erato* in bifurcating phylogenies, *H. hecalesia* shares variation with the clades of *Heliconius sara* and *Heliconius clysonymus*. Principal Component Analysis of variation in the autosomal SNPs within the *H. erato/sapho* clade. First two PCs account for over half of the variation. (B) Models of divergence history in the *H. erato/Heliconius telesiphe* group inferred by PHRAPL, where orange edges indicate gene flow. Models including up to five terms for coalescence, gene flow and variation in population sizes were fitted to four sets of three taxa, extracted from the 6725 gene trees. The bar in panel 4E shows time in units of $4N$ (diploid population size; see [supplementary table S6](#), [Supplementary Material](#) online).

heurippa (Salazar et al. 2008, 2010); admixture between *H. cydno/timareta* and subspecies of *H. melpomene* (Martin et al. 2013; Nadeau et al. 2013; Enciso-Romero et al. 2017); the

exchange between *H. melpomene*, *H. ethilla* group of silvaniforms, and ultimately *H. elevatus* (*Heliconius* Genome Consortium 2012; Wallbank et al. 2016). The fact that we

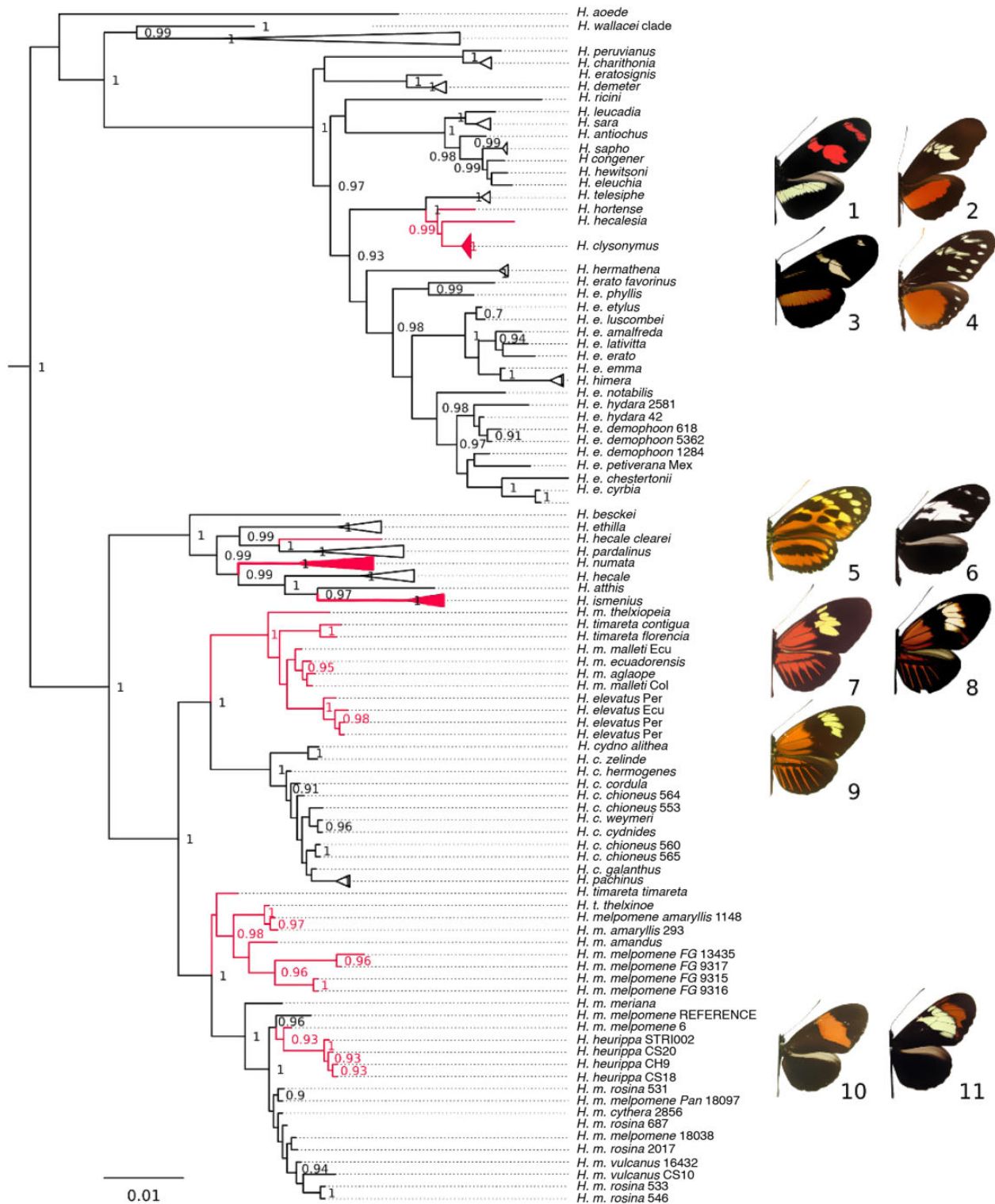


FIG. 5.—Discordance at the red patterning locus. Branches in positions varying from the species tree are labeled red. The ML tree was estimated for a 20 kb region on the *optix* scaffold (HE670865:360,000:380,000), containing the intervals most strongly associated with wing patterns in *Heliconius erato* and *Heliconius melpomene*. Intraspecific relations for species not discussed in text are collapsed. Outgroups and parametric support values <0.9 not shown. 1. *Heliconius telesiphe sotericus*, 2. *Heliconius hortense*, 3. *Heliconius clysonymus hygiana*, 4. *Heliconius hecalesia formosus*; 5. *Heliconius hecale felix*, 6. *Heliconius hecale clearei*; 7. *Heliconius timareta timareta*, 8. *Heliconius melpomene malleti*, 9. *Heliconius elevatus*; 10. *Heliconius melpomene melpomene*, 11. *Heliconius heurippa*.

Table 2Major Wing Pattern and Color Loci in *Heliconius*

<i>Heliconius Melpomene</i>	<i>Heliconius erato</i>	Other	Genes	Scaffold	Phenotype	Key References
B	D	<i>Br1G</i> ^a	<i>optix</i> , putative enhancers	HE670865	Red on HW and FW, ventral brown patterns	Reed et al. (2011), Supple et al. (2013), Van Belleghem et al. (2017), and Wallbank et al. (2016)
Yb/Sb/N	Cr	<i>P</i> ^b	<i>cortex</i> , putative enhancers, and possibly nearby genes.	HE667780	Yellow/white on HW and FW	Joron et al. (2006), Nadeau et al. (2016), Enciso-Romero et al. (2017), and Van Belleghem et al. (2017)
Ac	Sd		<i>WntA</i> , putative enhancers	HE668478 HE669520	Pattern shape	Martin et al. (2012) and Mazo-Vargas et al. (2017)
Ro	Ro		possibly <i>w1</i> or <i>rsp3</i>	HE671554	FW band shape	Morris et al. (2019) and Van Belleghem et al. (2017)
K	K		<i>aristaless2</i>	HE671246 HE670889	White/yellow switch	Westerman et al. (2018)

NOTE.—Color pattern loci are historically named differently in various species (Sheppard et al. 1985). However, more recent research has demonstrated that loci that have been defined from intraspecific crosses in different species map to homologous regions of the genome (e.g., see Joron et al. [2006]). Moreover, candidate protein-coding genes have been identified and, in some cases, the intervals containing functional variation have been localized (see Key References). Scaffold numbers refer to the *Hmel v1* assembly. HW, hindwing; FW, forewing.

^aBrown patterns in *Heliconius cydno* and *Heliconius pacheus* (Chamberlain et al. 2011).

^bThe *Pushmipullyu* supergene controlling most of the wing patterning in *Heliconius numata* (Joron et al. 2011).

can detect known events increases our confidence in the detection of additional instances across the radiation.

Inclusion of all species in the SEC clade made it possible to pinpoint the extensive admixture between *H. hecalesia* and 1) the ancestor of the *H. clysonymus* clade ($\gamma = 0.38$); 2) *H. clysonymus* itself ($\gamma = 0.16$). Adaptive gene flow between the three species is plausible, as *H. hecalesia* is sympatric with the other two species in parts of its range (Rosser et al. 2012). *H. clysonymus* \times *H. hecalesia* and *H. hortense* \times *H. hecalesia* hybrids have been found in the wild (Mallet et al. 2007). To a lesser extent, some degree of gene flow is certain between *H. clysonymus* and *H. sara* clades, although even with rich data it remains difficult to reconstruct specific events when several recently diverged species are involved, as the exact parameter values in the coalescent models depend on the sampling of taxa (fig. 4D and E). The problem is especially acute in the reconstruction of introgression histories at the wing pattern loci, where no specific topology is strongly supported, and even top-scoring networks are difficult to interpret given the differences in wing phenotypes of putatively introgressing species (fig. 5:1–4 and supplementary figs. 12–14, [Supplementary Material](#) online). As variation in *Heliconius* wing patterns appears to be governed by short regulatory elements that differ even between mimics (Concha et al. 2019), detailed investigation will be necessary to identify the specific functional regions within the broader intervals investigated here. Nonetheless, *Heliconius* are unusual in that introgression of

unlinked loci enables rapid evolution of complex patterns, which comprise a patchwork of elements sometimes derived from different sources (Wallbank et al. 2016). Many genomic studies of interspecific gene flow have found introgressions of small genome regions driven by natural selection on beneficial alleles, such as multiple abiotic tolerance factors in *Helianthus debilis* into *Helianthus annuus* (Whitney et al. 2010), the hypoxia resistance *EPAS1* haplotype (Denisovans \rightarrow anatomically modern Tibetans) (Huerta-Sánchez et al. 2014), the *ALX1* alleles determining diverse beak shapes among Darwin's finches (*Geospiza*) (Lamichhaney et al. 2015), or the *Agouti* variant conferring protective coat color (*Lepus americanus* \rightarrow *Lepus timidus*) (Giska 2019). Only in a few other systems is there evidence for adaptive introgression at multiple loci, including hominins (reviewed by Gokcumen 2020), and the *Lonchura* finches (Stryjewski and Sorenson 2017). Similar to *Lonchura*, the evolution of the key adaptive trait in *Heliconius* (patterning) has involved introgressions at multiple loci and between different combinations of species.

Challenges of Inferring Interspecific Gene Flow

While admixture is rampant, it remains difficult to describe it with precision. Even though all approaches suggest that gene flow occurred, the exact sources and direction are not estimated consistently between methods. The PhyloNet maximum pseudolikelihood (MPL) networks contain 13 reticulation edges (fig. 2), five of which are also recovered

by the TreeMix AG (fig. 3): *H. hecalesia*—*CHT* clade; *H. hecalesia*—*H. erato*; *H. melpomene*—*H. timareta*; *H. melpomene*—*H. cydno*; *H. melpomene* clade—silvaniforms. The TreeMix AG does not detect the exchanges in and between the small *H. egeria* and *H. hecuba* clades, or some of the events previously documented between species of the silvaniform group and *H. melpomene* (Jay et al. 2018; Zhang et al. 2016). The discrepancies are expected between two widely different techniques, as the TreeMix AG algorithm assumes that the underlying sequence of events was largely tree-like (Pickrell and Pritchard 2012). The AG approach, based on allele frequencies, was designed with assumptions more appropriate at the level of recently diverged taxa and may be affected by issues of multiple substitution. Similarly, the presented *D* statistics need to be taken with caution. Although the factors affecting the specificity of *D* have not been formally determined, it is likely to be affected in clades more distant from the *H. melpomene* reference genome, as worse read mapping results in lower overall number of sites for comparison (supplementary table 3, [Supplementary Material](#) online) and thus possibly an unfavorable signal-to-noise ratio. In comparison, the sensitivity of the *D* statistic decreases both when the population size is large relative to the divergence time, as is the case for many widespread *Heliconius* species, and when gene flow was ancient (Zheng and Janke 2018). More surprising is the disparity between two approaches computing over gene trees, MPL networks and PHRAPL. In case of the latter, the ability to evaluate a large number of models with an extensive data set of thousands of gene trees comes at the cost of less accurate parameter estimates, e.g. when compared with Approximate Bayesian Computation approaches (Jackson et al. 2017). Furthermore, the computational burden is reduced by limiting the questions to rooted triplets of taxa and subsampling intraspecific allelic diversity, thus losing many of the benefits of comprehensive sampling.

Other recent studies of introgression among *Heliconius* encountered similar difficulties. For instance, an analysis of whole genomes of 20 species (Edelman et al. 2019) identified the same key patterns (e.g., uncertain placement of *H. hecalesia*; gene flow *H. hecalesia*—*CHT*; *H. melpomene*—silvaniforms), but with overall low confidence and without the ability to ascertain if the proposed events involved unobserved lineages. Recent application of full likelihood coalescent modeling produced more robust results (Thawornwattana et al. 2021), but included only six out of 20 species in the SEC clade, making it impossible to infer the exact sources of admixture. The representation of intraspecific variation is also important: in our study we sample only the nonmimetic *H. hermathena hermathena* and thus cannot replicate the results of Massardo et al. (2020), who discovered introgression at *cortex* between *H. erato* and its mimic *H. hermathena ver-eatta*. Despite the difficulties in matching sufficient data with robust analytical tools, all approaches used in our and other studies point to *H. hecalesia* as a product of hybridization.

Neither Concatenation nor Coalescent Trees Adequately Represent Species History

There has been a marked shift over recent years away from phylogenetic methods that involve concatenation of data, and toward approaches that involve coalescent modeling. Methods for inferring a species tree by modeling the incomplete sorting of loci represent an improvement on the assumption that there is a common evolutionary history across all genomic regions (Heled and Drummond 2010; Liu et al. 2010; Mirarab et al. 2014), although the variation in results demonstrates the need for better analytical tools, as well as more complete data. Across the tree of life, from birds (Reddy et al. 2017) and mammals (Chen et al. 2017) to land plants (Zhong et al. 2013) and fungi (Shen et al. 2016), treatment of individual gene trees under MSC methods has yielded substantially different results to simple concatenation. In contrast, our *Heliconius* trees are consistent with previous work (Beltran et al. 2007; Kozak et al. 2015; Zhang et al. 2016; Edelman et al. 2019), but clarify some uncertainties, including the placement of the *H. hecuba* and *H. egeria* groups, relationships in the *H. sapho* clade, and the position of *H. besckei*. Nonetheless, similar to other large phylogenetic studies (Brawand et al. 2014; Fontaine et al. 2015), none of the individual gene trees showed exactly the same topology as the autosomal MP-EST species tree, suggesting that the well-supported bifurcating trees do not fully represent the underlying signal in the genomes within this clade. Network modeling clearly demonstrates that introgression has been important throughout the evolution of the genus, and yet this process could easily be overlooked with many of the modern phylogenomic methods.

The comprehensive analysis of the large butterfly genus shows the important role of adaptive introgression at multiple loci in shaping radiations. The main appeal of studying adaptive radiations is their power for analyzing trait evolution in a comparative framework, and a growing number of studies are looking at several *Heliconius* characters through this lens (e.g., Briscoe et al. 2013; Sculfort et al. 2020). It is increasingly clear that many key adaptive traits are determined by introgressed sequences, and thus a comparative approach reliant on a single bifurcating species tree would give highly incomplete results (Hahn and Nakhleh 2016; Bastide et al. 2018). To expose the hidden uncertainties of phylogeny and capture the potential of adaptations to be shared between species, future work must utilize approaches that reflect the nonbifurcating reality of evolving genomes.

Materials and Methods

Sampling

Heliconius can be divided into two deep lineages (fig. 1 and [supplementary file 1, Supplementary Material](#) online). The first consists of *H. erato*, *H. sara*, *H. clysonymus* and relatives,

and throughout the text we refer to this group as *SEC*. This lineage can be subdivided into three smaller clades of species closely related to *H. sara*, *H. erato*, and *H. clysonymus*. The clade of *H. clysonymus*, *H. hortense*, and *H. telesiphe* turned to be of special interest and we refer to it as *CHT*. The second major lineage within the genus are species related to *H. melpomene*, divided into five groups: the *H. melpomene/H. cydno* group; *H. numata* and relatives, often called “silvaniforms”; and the clades of *H. doris*, *H. wallacei*, and *H. aoede*. The first two clades are often grouped together and referred to as the *H. melpomene/cydno/silvaniform* clade (*MCS*).

We sampled 40 out of 47 *Heliconius*, as well six of the 12 species in the sister genus *Eueides*, and the monotypic *Dryadula* and *Agraulis* as outgroups (supplementary file 1, Supplementary Material online). Genomes of 11 species were re-sequenced for the first time: *Heliconius atthis*, *Heliconius antiochus*, *Heliconius egeria*, *Heliconius leucadia*, *Heliconius peruvianus*, *Eueides aliphera*, *Eueides lampeto*, *Eueides lineata*, *Eueides isabella*, *Eueides vibilia*, *Agraulis vanillae*. Material of sufficient quality could not be obtained for the remaining seven species of *Heliconius* and six of *Eueides*. Data for the other 37 species included in the study were published previously (*Heliconius Genome Consortium* 2012; Briscoe et al. 2013; Kronforst et al. 2013; Martin et al. 2013; Supple et al. 2013; Nadeau et al. 2016; Wallbank et al. 2016; Enciso-Romero et al. 2017; Jay et al. 2018). To enhance coalescent modeling by sampling genetic diversity (Edwards et al. 2016), we included individuals from distant populations and diverse wing pattern races when possible. Our full data set totaled 145 individuals and included multiple individuals of most species.

DNA Sequencing

All sequencing data used in this study, novel and previously published, were generated with the Illumina technology with 100 bp paired-end reads, insert sizes of 250–500 bp and read coverage from 12× to 110×. In case of the new samples, DNA was extracted with the DNeasy Blood and Tissue kit (Qiagen) from 30 to 50 μg of thorax tissue homogenized in buffer ATL using the TissueLyser (Qiagen); purified by digesting with RnaseA (Qiagen); and quantified on a Qubit v.1 spectrophotometer (LifeTechnologies). Whole genome libraries with an average insert size of 500 bp were sequenced on a HiSeq 2500 to a mean coverage depth of 50.7× (range: 33.1–67.8×).

Read Mapping and Genotyping

Raw reads were checked using FastQC v0.11 (Andrews 2014) and aligned to the *H. melpomene melpomene* reference v1 (*Heliconius Genome Consortium* 2012) with BWA v6 (Li and Durbin 2009). Initial BWA alignments were improved with Stampy v1.0.18 (Lunter and Goodson 2011). Aligner

parameters were based on earlier empirical tests (Davey 2013; Nadeau et al. 2013) and the age of divergence from the reference (Kozak et al. 2015) (supplementary table 2, Supplementary Material online). Alignments were sorted with Samtools (Li et al. 2009), deduplicated with Picard v1.112 (Fennell 2010) and re-aligned in Genome Analysis Toolkit v3.1 (GATK) (McKenna et al. 2010; DePristo et al. 2011). SNPs were called separately across samples at sites with coverage >4× and quality >20 using the GATK Unified Genotyper (van der Auwera et al. 2013). Species genotypes were merged using Bcftools v1 (Li et al. 2009) and assessed with an in-house Python script (Martin et al. 2013) (evaluateVCF-03.py [Martin 2017]). We identified 126,865,683 individual SNPs (supplementary table 3, Supplementary Material online), including 5,483,419 in the exome. The autosomal matrix of exonic, biallelic, nonsingleton SNPs genotyped in all individuals contained 122,913 variants. Commands for genotyping and phylogenetic software are given in the Supplementary Methods.

Exome Alignments and Gene Trees

Protein-coding genes can be effectively treated as discrete markers for multilocus phylogenetics (Edwards et al. 2016). Exonic markers were chosen over noncoding loci because 1) reads from distantly related species map better at the CDS; 2) orthologous sequences can be identified with greater confidence. We minimized paralogy by narrowing the gene set to 1:1:1 orthologs between *H. melpomene*, *Danaus plexippus*, and *Bombyx mori* identified by OrthoMCL (Li et al. 2003; *Heliconius Genome Consortium* 2012). Alignments of entire protein-coding, single-copy genes were extracted with an in-house script (gene_fasta_from_reseq.py [Martin 2017]). For this analysis, we ignored all genes within scaffolds linked to the color pattern loci (see table 2), as the exact boundaries of these loci have not been established for most species (Van Belleghem et al. 2017) and linkage to loci involved in adaptive color pattern differences might mislead phylogenetic inference.

We trimmed the alignments with TrimAl v1.2 (Capella-Gutiérrez et al. 2009), removing any sequences that contained >50% missing data (see the command line in Supplementary Methods). Furthermore, high entropy sections of each alignment were excluded by Block Mapping and Gathering with Entropy (BMGE) (Crisuolo and Gribaldo 2010) with a moderately relaxed PAM100 similarity matrix. Individual ML gene trees were estimated in FastTree v2.1 (Price et al. 2010) with parametric aLRT nodal support (Anisimova and Gascuel 2006). Species tree and network analyses listed below were conducted using rooted gene trees inferred from the 6,725 autosomal and 406 sex-linked CDS genes.

Incongruence in the Data

To assess how much the topologies of gene trees differ from one another, we calculated the Robinson–Foulds distance (RF) (Robinson and Foulds 1981) for all pairs of trees, normalized by dividing the observed distance by the maximum possible RF between the two trees. This statistic was calculated using PAUP* v4 (Swofford 2002) across the entire data set of 145 samples and 6725 genes. As some of the differences are expected to arise from the lack of intraspecific resolution, the calculation was repeated on a thinned data set of 57 high coverage individuals representing all species, with additional individuals included in species with strong geographic structure (supplementary file 1, Supplementary Material online).

We identified highly incongruent nodes by computing 50% majority rule trees and using four information-theory measures (Salichos and Rokas 2013; Salichos et al. 2014) on the reduced data set of 57 samples at 6,725 genes. These analyzes were performed in RAxML v8 (Stamatakis 2014). The information-theory measures included the: 1) IC, which compares the frequency of a bipartition to the frequency of the most common alternative; 2) the IC All (ICA), which considers all alternatives with support $\geq 5\%$; 3) the corresponding tree certainty (TC), calculated and normalized over all bipartitions; and 4) the tree certainty All (TCA) (Salichos et al. 2014). All four measures are expressed on a scale from -1 (when the bipartition is not found in any of the gene trees) to 1 (when the bipartition is found in all). Because various patterns of missing data can impact the IC/TC values (Salichos et al. 2014), and many of our gene trees are incompletely resolved, we examined the impact of input data quality on these scores by repeating the procedure with the 1,000 most resolved phylogenies.

Species Trees

Naïve “total evidence” phylogenies were estimated from concatenated exonic SNPs in RAxML v8 with 100 bootstrap replicates, GTR+ Γ model and ascertainment bias correction (Stamatakis 2014). The history of the matriline was approximated from the whole-mitochondrial alignment with partitions determined by PartitionFinder v1.1 (Lanfear et al. 2012). In addition, we used two MSC approaches to estimate the species tree under the assumption of Incomplete Lineage Sorting. MP-EST v1.4 maximizes a pseudo-likelihood function over the distribution of taxon triples extracted from gene tree topologies, and provides a measure of incongruence based on the proportion of triples shared by the gene trees, similar to the RF distance (Liu et al. 2010). An MSC phylogeny was inferred in MP-EST from the 6,725 gene trees, evaluating support by re-estimating the tree 100 times with random samples of 500 gene trees. Since MP-EST may be misled by errors in gene tree reconstruction (Mirarab and Warnow 2015), we compared the results with ASTRAL-III, a fast quartet

method that accounts for polytomies and low support values in the input (Zhang et al. 2017). ASTRAL quantifies discordance by computing how many of the gene trees contain the quartets making up the species tree (Sayyari and Mirarab 2016).

Recombination between exons scattered across a long genomic interval may lead to conflicting signals, which could be obscured by performing phylogenetic inference at the level of a complete coding gene, a practice criticized as “concatalescence” (Gatesy and Springer 2013). To account for this possibility, we repeated the ASTRAL-III species tree inference using individual autosomal exons longer than 500 base pairs. By restricting analysis to these 6,367 longer exons, we ensured sufficient information content, while eliminating the possibility that recombination between exons of one gene was responsible for conflicting signals.

Admixture Networks

Following the identification of problematic nodes based on gene tree statistics, information criteria and conflicting nodes in species trees, we applied two distinct network approaches (Hahn and Nakhleh 2016). First, we determined the admixture graph (AG) in TreeMix v1.13 by identifying the pairs of taxa sharing more than the expected proportion of allelic variation (Pickrell and Pritchard 2012). Individuals were again assigned to taxa, distinguishing major clades within well-represented species as separate lineages. Relations between taxa were inferred from allele frequency data computed in PLINK v1.9 (Chang et al. 2015), based on the matrix of autosomal SNPs. As TreeMix assumes individual SNPs to be represented across samples and independent, the original matrix was filtered to remove sites with $<95\%$ complete data. We identified and pruned sites that could be linked within species, using the pairwise linkage disequilibrium estimator in PLINK v1.9 with default settings.

Second, we modeled both hybridization and incomplete lineage sorting under the MSC network framework implemented in PhyloNet v3.5. Networks were computed under the MPL criterion from the 6725 rooted autosomal phylogenies, considering only nodes with support >0.8 ($-b 0.8$) and starting with the MP-EST species tree. To search for ancient admixtures between deeper branches of the tree, we conducted an analysis with one species from each of the seven *Heliconius* clades (*H. melpomene*, *H. numata*, *H. doris*, *H. wallacei*, *H. erato*, *H. telesiphe*, *H. aoede*) and *Eueides*, as a full run with all the samples was not feasible. The optimal network was determined by calculating the Bayesian information criterion from the maximum likelihood and the number of lineages, admixture edges and gene trees in each model (supplementary file 3, Supplementary Material online) (Yu et al. 2014).

Gene Flow in the *H. erato* Lineage

Admixture has been studied only in a few species of the *SEC* clade (Edelman et al. 2019; Massardo et al. 2020). Here, we focused on the events involving *H. hecalesia*, *H. clysonymus* and cognates. The extent of genome-wide similarity between species clusters was illustrated with PCAs of variation in the matrix of autosomal SNPs, calculated for the *SEC* clade in the R package *adegenet* (Jombart and Ahmed 2011). To test for gene flow we calculated the *D* statistic (Durand et al. 2011), derived from the allelic configurations of two taxa, P_1 and P_2 , their relative P_3 and an outgroup. Under the null hypothesis, no admixture occurred between P_3 and either P_1 or P_2 . Under the alternative, P_3 exchanged alleles with either P_1 or P_2 , resulting in the excess of the corresponding allelic configuration. Significance of the result can be assessed by block jackknifing (Martin et al. 2015). Specific tests were conducted for gene flow between *H. hecalesia* (P_2) and *H. clysonymus*, *H. hortense*, *H. telesiphe* or species from the *H. sara* clade (P_3). The sister species P_1 was either the allopatric *H. erato* from French Guiana, or the parapatric *H. erato* from Amazonia, and the outgroup was always *H. melpomene*.

To address the hypothesis of hybrid origin of *H. hecalesia* or the *H. clysonymus/H. hortense* pair explicitly, we modeled various scenarios of divergence with gene flow under the maximum likelihood criterion as implemented in PHRAPL (Jackson et al. 2017). PHRAPL is a maximum likelihood method to assess complex scenarios including lineage coalescence, gene flow and population growth. PHRAPL uses simulations to compare all possible scenarios under a range of parameter values sampled from a predefined grid, using gene tree topology as the summary statistic (Jackson et al. 2017). We fitted models of speciation history to four distinct triplets of taxa: 1) *H. erato* (Western and Andean populations), *H. hecalesia* and *H. clysonymus* (including the sister species *H. hortense*); 2) *H. telesiphe*, *H. clysonymus* and *H. charithonia* (including the sister species *H. peruvianus*); 3) *H. erato*, *H. hecalesia* and *H. telesiphe*; 4) *H. telesiphe*, *H. charithonia* and *H. sara*. The four sets of taxa were chosen based on the earlier evidence for introgression from either MPL networks and TreeMix (1, 2) or the *D* statistics (1–4). To diminish the computational burden, we subsampled up to three tips per species from the 6,725 gene trees with 30 replicates per tree (Jackson et al. 2017). For each triplet, we evaluated a total of 48 models, including parameters for coalescence, symmetric migration, and change in population size between lineages, estimated at the default values for a PHRAPL grid search. The optimal model was selected by weighted Akaike's information criterion (wAIC).

Introgression at the Color Pattern Loci

The history of the loci associated with aposematic wing phenotypes is distinct due to strong selection (Möst et al. 2020), and thus the seven scaffolds in the *Hmel v1* assembly

containing these loci (table 2) were treated separately. Each scaffold alignment was partitioned into windows of 20 kb, sliding by 10 kb, discarding windows with <1000 polymorphic sites [script *sliphy3.py* (Martin 2017)]. The topology for every window was reconstructed and tested for significant differences from the MP-EST species tree using the SH test (Shimodaira and Hasegawa 1999) in RAXML. In order to understand precisely how the *Hmel v1* reference corresponds to the specific red control loci of *H. erato* (Supple et al. 2013), the *optix* (*B/D*) scaffold HE670865 was aligned against the *H. erato* *B/D* BACs (Papa et al. 2008) with mLAGAN (Brudno et al. 2003).

After finding discordant topologies at the *optix*, *cortex*, and *WntA* loci, we tested if the variation can be explained by incomplete lineage sorting alone, or whether gene flow in the *SEC* clade needs to be taken into account. We focused on specific intervals around the key genes, where departures from the species tree were found for *SEC*: HE670865:310,000:460,000, containing the *optix* protein CDS and several regulatory elements (Supple et al. 2013; Van Belleghem et al. 2017); HE667780:570000:750000, including *cortex* (Nadeau et al. 2016; Van Belleghem et al. 2017) and the novel inversion identified in some species of the *SEC* clade (Edelman et al. 2019); HE668478:450,000:500,000, containing *WntA* (table 2).

We analyzed all three genomic intervals separately under coalescent models in BEAST2. In each case, the interval was divided into windows of 10 kb treated as separate partitions, and the alignments were reduced to the relevant species: *H. hecalesia*; the *CHT* clade; *H. sara* and *H. charithonia*; *H. erato*, *H. himera* and *H. hermathena*. First, the coalescent tree model, where incongruence is purely due to incomplete lineage sorting, was fitted in StarBEAST2 (Ogilvie et al. 2017). Each partition was assigned the HKY+ Γ substitution model with four rate categories, and a speciation-only tree model was selected for compatibility with the species network analysis. Based on the age of the *Eueides-Heliconius* split (Chazot et al. 2019), we used a strict molecular clock with an estimated exome-wide rate of 0.003 substitutions per site per MY. Two independent chains of 200 million cycles with 50% burnin were executed for each analysis; possible bias in priors was assessed by executing empty prior runs; and the convergence and effective sample sizes of the numeric parameters were visualized in Tracer (Rambaut et al. 2014). Second, the coalescent network was estimated in BEAST2 (Zhang et al. 2018): a model where incongruence can be a result of either ILS or admixture between species. Additional priors included: species net diversification rate (exponential with mean 1.0, corresponding to doubling every 1 My) and turnover rate (beta distribution: $\alpha = 3.0$; $\beta = 1.0$, corresponding to low probability of admixture). The relative fit of the tree and network models to the same data was estimated by computing Bayes Factors from marginal likelihoods determined by Path Sampling with 20 steps and chains of 10 million cycles

(Baele et al. 2013). Networks were visualized in IcyTree (Vaughan 2017).

Supplementary Material

Supplementary data are available at *Genome Biology and Evolution* online.

Acknowledgments

This study was supported by the European Research Council Grant [339873 to C.J.]; French ANR Grant HYBEVOL (ANR-12-JSV7-0005 to M.J.); Smithsonian Institution funding [to W.O.M.]; and Herchel Smith, Cambridge Philosophical Society and Panton Trust grants [to K.M.K.].

We thank the governments of Peru, Ecuador, and Suriname for permits to collect butterflies. Kanchon Dasmahapatra, James Mallet, and Camilo Salazar provided advance access to genomic data and helpful comments. Analyses were conducted on a machine made available by Aylwyn Scally, clusters at the School of Life Sciences, University of Cambridge operated with help from Jenny Barna, and the STRI Plato server run by Eugenio Valdes. Richard Nichols and John Welch examined an early draft of the manuscript. We also thank Luay Nakhleh and five anonymous reviewers for their constructive criticism.

Data Availability

The SNP calls, DNA alignments, and gene trees can be downloaded from a public repository (<https://doi.org/10.6084/m9.figshare.c.4837116.v1>). Novel Illumina sequence data are available on the EBI Short Read Archive under the accession numbers ERS5668103–ERS5668111 and ERS5551469–ERS5551479.

Literature Cited

- Andrews S. 2014. FastQC. <http://www.bioinformatics.babraham.ac.uk/projects/fastqc/>. [accessed 2014 July 1]
- Anisimova M, Gascuel O. 2006. Approximate likelihood-ratio test for branches: a fast, accurate, and powerful alternative. *Syst Biol*. 55(4):539–552.
- Baele G, Li WLS, Drummond AJ, Suchard MA, Lemey P. 2013. Accurate model selection of relaxed molecular clocks in Bayesian phylogenetics. *Mol Biol Evol*. 30(2):239–243.
- Bastide P, Solís-Lemus C, Kriebel R, William Sparks K, Ané C. 2018. Phylogenetic comparative methods on phylogenetic networks with reticulations. *Syst Biol*. 67(5):800–820.
- Beltran M, et al. 2007. Do pollen feeding, pupal-mating and larval gregariousness have a single origin in Heliconius butterflies? Inferences from multilocus DNA sequence data. *Proc R Soc B*. 92:221–239.
- Brawand D, et al. 2014. The genomic substrate for adaptive radiation in African cichlid fish. *Nature* 513(7518):375–381.
- Briscoe AD, et al. 2013. Female behaviour drives expression and evolution of gustatory receptors in butterflies. *PLoS Genet*. 9(7):e1003620.
- Brower AVZ, Garzón-Orduña JJ. 2018. Missing data, clade support and “reticulation”: the molecular systematics of Heliconius and related genera (Lepidoptera: Nymphalidae) re-examined. *Cladistics* 34(2):151–166.
- Brudno M, et al. 2003. LAGAN and Multi-LAGAN: efficient tools for large-scale multiple alignment of genomic DNA. *Genome Res*. 13(4):721–731.
- Capella-Gutiérrez S, Silla-Martínez JM, Gabaldón T. 2009. trimAl: a tool for automated alignment trimming in large-scale phylogenetic analyses. *Bioinformatics* 25(15):1972–1973.
- Chamberlain NL, Hill RI, Baxter SW, Jiggins CD, Kronforst MR. 2011. Comparative population genetics of a mimicry locus among hybridizing *Heliconius* butterfly species. *Heredity (Edinb)*. 107(3):200–204.
- Chang CC, et al. 2015. Second-generation PLINK: rising to the challenge of larger and richer datasets. *Gigascience* 4:7.
- Chazot N, et al. 2019. Priors and posteriors in Bayesian timing of divergence analyses: the age of butterflies revisited. *Syst Biol*. 68(5):797–813.
- Chen M-Y, Liang D, Zhang P. 2017. Phylogenomic resolution of the phylogeny of Laurasiatherian mammals: exploring phylogenetic signals within coding and noncoding sequences. *Genome Biol Evol*. 9(8):1998–2012.
- Concha C, et al. 2019. Interplay between developmental flexibility and determinism in the evolution of mimetic *Heliconius* wing patterns. *Curr Biol*. 29(23):3996–4009.
- Crisuolo A, Gribaldo S. 2010. BMGE (Block Mapping and Gathering with Entropy): a new software for selection of phylogenetic informative regions from multiple sequence alignments. *BMC Evol Biol*. 10:210.
- Cui R, et al. 2013. Phylogenomics reveals extensive reticulate evolution in *Xiphophorus* fishes. *Evolution* 67(8):2166–2179.
- Dasmahapatra KK, et al. 2007. Genetic analysis of a wild-caught hybrid between non-sister *Heliconius* butterfly species. *Biol Lett*. 3(6):660–663.
- Davey JW. 2013. heliconius.org: Aligning Heliconius short read sequences. [accessed 2013 May 1]. Available from: <http://www.heliconius.org/2013/aligning-heliconius-short-read-sequences/>.
- Degnan JH. 2018. Modeling hybridization under the network multispecies coalescent. *Syst Biol*. 67(5):786–799.
- DePristo MA, et al. 2011. A framework for variation discovery and genotyping using next-generation DNA sequencing data. *Nat Genet*. 43(5):491–498.
- Durand EY, Patterson N, Reich D, Slatkin M. 2011. Testing for ancient admixture between closely related populations. *Mol Biol Evol*. 28(8):2239–2252.
- Edelman NB, et al. 2019. Genomic architecture and introgression shape a butterfly radiation. *Science* 366(6465):594–599.
- Edwards SV, Potter S, Schmitt CJ, Bragg JG, Moritz C. 2016. Reticulation, divergence, and the phylogeography–phylogenetics continuum. *Proc Natl Acad Sci USA*. 113(29):8025–8032.
- Enciso-Romero J, et al. 2017. Evolution of novel mimicry rings facilitated by adaptive introgression in tropical butterflies. *Mol Ecol*. 26(19):5160–5172.
- Feliner GN, et al. 2017. Is homoploid hybrid speciation that rare? An empiricist’s view. *Heredity* 118:513–516.
- Fennell T. 2010. Picard Tools. broadinstitute.github.io/picard. [Accessed 2014 July 1]
- Fontaine MC, et al. 2015. Extensive introgression in a malaria vector species complex revealed by phylogenomics. *Science* 347(6217):1258524.
- Gatesy J, Springer MS. 2013. Concatenation versus coalescence versus ‘concatalescence’. *Proc Natl Acad Sci USA*. 110(13):E1179.
- Giska I, et al. 2019. Introgression drives repeated evolution of winter coat color polymorphism in hares. *Proc Natl Acad Sci U S A*. 116(48):24150–24156.
- Gokcumen O. 2020. Archaic hominin introgression into modern human genomes. *Yearbook Phys Anthropol*. 171(S70):60–73.

- Hahn MW, Nakhleh L. 2016. Irrational exuberance for resolved species trees. *Evolution* 70(1):7–17.
- Heled J, Drummond AJ. 2010. Bayesian inference of species trees from multilocus data. *Mol Biol Evol.* 27(3):570–580.
- Heliconius Genome Consortium. 2012. Islands of divergence underlie adaptive radiation in a butterfly genome. *Nature* 487:94–98.
- Hilario E, Gogarten JP. 1993. Horizontal transfer of ATPase genes—the tree of life becomes a net of life. *Biosystems* 31(2–3):111–119.
- Huerta-Sánchez E, et al. 2014. Altitude adaptation in Tibetans caused by introgression of Denisovan-like DNA. *Nature* 512:194–197.
- Jackson ND, Morales AE, Carstens BC, O’Meara BC. 2017. PHRAPL: phylogeographic inference using approximate likelihoods. *Syst Biol.* 66(6):1045–1053.
- Jay P, et al. 2018. Supergene evolution triggered by the introgression of a chromosomal inversion. *Curr Biol.* 28(11):1839–1845.e3.
- Jombart T, Ahmed I. 2011. adegenet 1.3-1: new tools for the analysis of genome-wide SNP data. *Bioinformatics* 27(21):3070–3071.
- Joron M, et al. 2006. A conserved supergene locus controls colour pattern diversity in *Heliconius* butterflies. *PLoS Biol.* 4(10):e303.
- Joron M, et al. 2011. Chromosomal rearrangements maintain a polymorphic supergene controlling butterfly mimicry. *Nature* 477(7363):203–206.
- Kang JH, Scharlt M, Walter RB, Meyer A. 2013. Comprehensive phylogenetic analysis of all species of swordtails and platies (Pisces: genus *Xiphophorus*) uncovers a hybrid origin of a swordtail fish, *Xiphophorus monticolus*. *BMC Evol Biol.* 13:25.
- Kozak KM, et al. 2015. Multilocus species trees show the recent adaptive radiation of the mimetic heliconius butterflies. *Syst Biol.* 64(3):505–524.
- Kronforst MR, et al. 2013. Hybridization reveals the evolving genomic architecture of speciation. *Cell Rep.* 5(3):666–677.
- Lamichhaney S, et al. 2015. Evolution of Darwin’s finches and their beaks revealed by genome sequencing. *Nature* 518(7539):371–375.
- Lanfear R, Calcott B, Ho SYW, Guindon S. 2012. Partitionfinder: combined selection of partitioning schemes and substitution models for phylogenetic analyses. *Mol Biol Evol.* 29(6):1695–1701.
- Li H, Durbin R. 2009. Fast and accurate short read alignment with Burrows–Wheeler transform. *Bioinformatics* 25(14):1754–1760.
- Li H, et al. 2009. The Sequence Alignment/Map format and SAMtools. *Bioinformatics* 25(16):2078–2079.
- Li L, Stoeckert CJ, Roos DS. 2003. OrthoMCL: identification of ortholog groups for eukaryotic genomes. *Genome Res.* 13(9):2178–2189.
- Liu L, Yu L, Edwards SV. 2010. A maximum pseudo-likelihood approach for estimating species trees under the coalescent model. *BMC Evol Biol.* 10:302.
- Lunter G, Goodson M. 2011. Stampy: a statistical algorithm for sensitive and fast mapping of Illumina sequence reads. *Genome Res.* 21(6):936–939.
- Mallet J, Beltran M, Neukirchen W, Linares M. 2007. Natural hybridization in heliconiine butterflies: the species boundary as a continuum. *BMC Evol Biol.* 7:28.
- Martin A, et al. 2012. Diversification of complex butterfly wing patterns by repeated regulatory evolution of a *Wnt* ligand. *Proc Natl Acad Sci USA.* 109(31):12632–12637.
- Martin SH. 2017. Genomics general scripts. <https://github.com/simonh-martin>. [Accessed 2019 March 1]
- Martin SH, Davey JW, Jiggins CD. 2015. Evaluating the use of ABBA-BABA statistics to locate introgressed loci. *Mol Biol Evol.* 32(1):244–257.
- Martin SH, et al. 2013. Genome-wide evidence for speciation with gene flow in *Heliconius* butterflies. *Genome Res.* 23(11):1817–1828.
- Massardo D, et al. 2020. The roles of hybridization and habitat fragmentation in the evolution of Brazil’s enigmatic longwing butterflies, *Heliconius nattereri* and *H. hermathena*. *BMC Biol.* 18(1):84.
- Mazo-Vargas A, et al. 2017. Macroevolutionary shifts of *WntA* function potentiate butterfly wing-pattern diversity. *Proc Natl Acad Sci USA.* 114(40):10701–10706.
- McKenna A, et al. 2010. The Genome Analysis Toolkit: a MapReduce framework for analyzing next-generation DNA sequencing data. *Genome Res.* 20(9):1297–1303.
- Mirarab S, et al. 2014. ASTRAL: genome-scale coalescent-based species tree estimation. *Bioinformatics* 30(17):i541–8.
- Mirarab S, Warnow T. 2015. ASTRAL-II: coalescent-based species tree estimation with many hundreds of taxa and thousands of genes. *Bioinformatics* 31(12):i44–i52.
- Moest M, et al. 2020. Selective sweeps on novel and introgressed variation shape mimicry loci in a butterfly adaptive radiation. *PLoS Biol.* 18(2):e3000597.
- Morris J, et al. 2019. The genetic architecture of adaptation: convergence and pleiotropy in *Heliconius* wing pattern evolution. *Heredity (Edinb.)* 123(2):138–152.
- Nadeau NJ, et al. 2013. Genome-wide patterns of divergence and gene flow across a butterfly radiation. *Mol Ecol.* 22(3):814–826.
- Nadeau NJ, et al. 2016. The gene cortex controls mimicry and crypsis in butterflies and moths. *Nature* 534(7605):106–110.
- Ogilvie HA, Bouckaert RR, Drummond AJ. 2017. StarBEAST2 brings faster species tree inference and accurate estimates of substitution rates. *Mol Biol Evol.* 34(8):2101–2114.
- Papa R, et al. 2008. Highly conserved gene order and numerous novel repetitive elements in genomic regions linked to wing pattern variation in *Heliconius* butterflies. *BMC Genomics* 9:345.
- Pardo-Diaz C, et al. 2012. Adaptive introgression across species boundaries in *Heliconius* butterflies. *PLoS Genet.* 8(6):e1002752.
- Pickrell JK, Pritchard JK. 2012. Inference of population splits and mixtures from genome-wide allele frequency data. *PLoS Genet.* 8(11):e1002967.
- Price MN, Dehal PS, Arkin AP. 2010. FastTree 2—approximately maximum-likelihood trees for large alignments. *PLoS One* 5(3):e9490.
- Rambaut A, Suchard M, Xie W, Drummond A. 2014. Tracer v. 1.6. <http://beast.bio.ed.ac.uk/>.
- Reddy S, et al. 2017. Why do phylogenomic data sets yield conflicting trees? Data type influences the avian tree of life more than taxon sampling. *Syst Biol.* 66(5):857–879.
- Reed RD, et al. 2011. *Optix* drives the repeated convergent evolution of butterfly wing pattern mimicry. *Science* 333(6046):1137–1141.
- Robinson DF, Foulds LR. 1981. Comparison of phylogenetic trees. *Math Biosci.* 53(1–2):131–147.
- Rosser N, Phillimore AB, Huertas B, Willmott KR, Mallet J. 2012. Testing historical explanations for gradients in species richness in heliconiine butterflies of tropical America. *Biol J Linn Soc.* 105(3):479–497.
- Roure B, Baurain D, Philippe H. 2013. Impact of missing data on phylogenies inferred from empirical phylogenomic data sets. *Mol Biol Evol.* 30(1):197–214.
- Salazar C, et al. 2010. Genetic evidence for hybrid trait speciation in heliconius butterflies. *PLoS Genet.* 6(4):e1000930.
- Salazar C, Jiggins CD, Taylor JE, Kronforst MR, Linares M. 2008. Gene flow and the genealogical history of *Heliconius heurippa*. *BMC Evol Biol.* 8:132.
- Salichos L, Rokas A. 2013. Inferring ancient divergences requires genes with strong phylogenetic signals. *Nature* 497(7449):327–331.
- Salichos L, Stamatakis A, Rokas A. 2014. Novel information theory-based measures for quantifying incongruence among phylogenetic trees. *Mol Biol Evol.* 31(5):1261–1271.
- Sayyari E, Mirarab S. 2016. Fast coalescent-based computation of local branch support from quartet frequencies. *Mol Biol Evol.* 33(7):1654–1668.
- Schumer M, Rosenthal GG, Andolfatto P. 2014. How common is homoploid hybrid speciation? *Evolution* 68(6):1553–1560.

- Sculfort O, et al. 2020. Variation of chemical compounds in wild Heliconiini reveals ecological and historical contributions to the evolution of chemical defences in mimetic butterflies. *Ecol Evol*. doi:10.1002/ece3.6044.
- Seixas FA, Edelman NB, Mallet J. 2021. Synteny-based genome assembly for 16 species of Heliconius butterflies, and an assessment of structural variation across the genus. *Genome Biology and Evolution*. Accepted.
- Shen X-X, et al. 2016. Reconstructing the backbone of the Saccharomycotina yeast phylogeny using genome-scale data. *G3 Genes, Genomes, Genet*. 6:3927–3939.
- Sheppard PM, Turner JRG, Brown KS, Benson WW, Singer MC. 1985. Genetics and the evolution of muellerian mimicry in Heliconius butterflies. *Philosophical Transactions of the Royal Society B*. 308(1137):433–610.
- Shimodaira H, Hasegawa M. 1999. Multiple comparisons of log-likelihoods with applications to phylogenetic inference. *DNA Seq*. 16(8):1114–1116.
- Stamatakis A. 2014. RAxML version 8: a tool for phylogenetic analysis and post-analysis of large phylogenies. *Bioinformatics* 30(9):1312–1313.
- Stryjewski KF, Sorenson MD. 2017. Mosaic genome evolution in a recent and rapid avian radiation. *Nat Ecol Evol*. 1(12):1912–1922.
- Supple MA, et al. 2013. Genomic architecture of adaptive color pattern divergence and convergence in *Heliconius* butterflies. *Genome Res*. 23(8):1248–1257.
- Swofford R. 2002. PAUP: Phylogenetic Analysis Using Parsimony (*and other methods). Available from: <http://phylosolutions.com/paup-test>. [Accessed 2016 June 1]
- Thawornwattana Y, et al. 2021. 'Complex introgression history of the erato-sara clade of Heliconius butterflies'. bioRxiv 10.1101/2021.02.10.430600.
- Van Belleghem SM, et al. 2017. Complex modular architecture around a simple toolkit of wing pattern genes. *Nat Evol Ecol*. 1:1–32.
- van der Auwera GA, et al. 2013. From fastq data to high-confidence variant calls: the Genome Analysis Toolkit best practices pipeline. *Curr Protoc Bioinform*. 43:1–33.
- Vaughan TG. 2017. IcyTree: rapid browser-based visualization for phylogenetic trees and networks. *Bioinformatics* 33(15):2392–2394.
- Wallbank RWR, et al. 2016. Evolutionary novelty in a butterfly wing pattern through enhancer shuffling. *PLoS Biol*. 14(1):e1002353.
- Wen D, Yu Y, Zhu J, Nakhleh L. 2018. Inferring phylogenetic networks using PhyloNet. *Syst Biol*. 67(4):735–740.
- Westerman EL, et al. 2018. Aristaless controls butterfly wing color variation used in mimicry and mate choice. *Curr Biol*. 28(21):3469–3474.e4.
- Whitney KD, Randell RA, Rieseberg LH. 2010. Adaptive introgression of abiotic tolerance traits in the sunflower *Helianthus annuus*. *New Phytol*. 187(1):230–239.
- Wiens JJ, Morrill MC. 2011. Missing data in phylogenetic analysis: reconciling results from simulations and empirical data. *Syst Biol*. 60(5):719–731.
- Yu Y, Dong J, Liu KJ, Nakhleh L. 2014. Maximum likelihood inference of reticulate evolutionary histories. *Proc Natl Acad Sci USA*. 111(46):11648–11653.
- Zhang C, Ogilvie HA, Drummond AJ, Stadler T. 2018. Bayesian inference of species networks from multilocus sequence data. *Mol Biol Evol*. 35(2):504–517.
- Zhang C, Sayyari E, Mirarab S. 2017. ASTRAL-III: increased scalability and impacts of contracting low support branches. In: RECOMB-CG 2017. Cham (Switzerland): Springer. p. 53–75.
- Zhang W, Dasmahapatra Kanchon K, Mallet J, Moreira GRP, Kronforst MR. 2016. Genome-wide introgression among distantly related *Heliconius* butterfly species. *Genome Biol*. 17:25.
- Zhang W, et al. 2019. Comparative transcriptomics provides insights into reticulate and adaptive evolution of a butterfly radiation. *Genome Biol Evol*. 11(10):2963–2975.
- Zheng Y, Janke A. 2018. Gene flow analysis method, the D-statistic, is robust in a wide parameter space. *BMC Bioinformatics* 19(1):10.
- Zhong B, Liu L, Yan Z, Penny D. 2013. Origin of land plants using the multispecies coalescent model. *Trends Plant Sci*. 18(9):492–495.

Associate editor: Davide Pisani